PNAS RESEARCH ARTICLE | CELL BIOLOGY

Mutant *IDH1* cooperates with *NPM1c* or *FLT3*^{ITD} to drive distinct myeloid diseases and molecular outcomes

Takashi Sakamoto[a,b,1], Julie Leca[a,c,1], Xin Zhang[a,1], Cem Meydan[d,e,f,g,2], Jonathan Foox[d,e,2], Parameswaran Ramachandran[a], Liam D. Hendrikse[a], Wenjing Zhou[a], Thorsten Berger[a], Jerome Fortin[a,h], Steven M. Chan[a], Ming-Feng Chiang[a], Satoshi Inoue[a,i], Wanda Y. Li[a,j], Mandy F. Chu[a], Gordon S. Duncan[a], Andrew Wakeham[a], François Lemonnier[a,k], Chantal Tobin[a], Ryan Mcwilliam[a], Isabelle Colonna[a], Christophe Bontoux[a,l], Soode Moghadas Jafari[a], Robert L. Bowman[m], Brandon Nicolay[n], Sebastien Ronseaux[n], Rohini Narayanaswamy[n], Ross L. Levine[m,o,p], Ari M. Melnick[g], Christopher E. Mason[d,e,f], Mark D. Minden[a], and Tak W. Mak[a,j,q,3]

Affiliations are included on p. 11.

Contributed by Tak W. Mak; received December 6, 2024; accepted April 6, 2025; reviewed by John Dipersio and Craig T. Jordan

In human acute myeloid leukemia (AML), mutations of isocitrate dehydrogenase-1 (*IDH1*) often co-occur with *NPM1* mutations, and less frequently with *FLT3* mutations. To investigate whether the effects of *IDH1* mutation differ according to the specific co-occurring mutation, we generated two strains of double knock-in mutant mice. *Idh1*^{R132H} combined with *Npm1c* induced overt AML, whereas *Idh1*^{R132H} plus *Flt3*^{ITD} resulted in *Flt3*^{ITD}-driven myelo- or lymphoproliferation that was minimally affected by *Idh1*^{R132H} and rarely generated AML. Gene expression profiling revealed differences between *Idh1*^{R132H};*Npm1c* cells and *Idh1*^{R132H};*Flt3*^{ITD} cells and suggested altered heme metabolism and immune responses in the former. The profile of *Idh1*^{R132H};*Npm1c* cells corresponded to that of human *IDH*-mutated AML cells, particularly those resistant to inhibitors of mutant IDH. Compared to treatment with a menin inhibitor, IDH1-targeted therapy of *Idh1*^{R132H};*Npm1c* AML-bearing mice was less efficacious in improving cell differentiation and extending survival. The differential cooperation of *Idh1*^{R132H} with *Npm1c* vs. *Flt3*^{ITD} may have implications for the devising of subtype-specific treatments for human AML.

IDH1 | NPM1 | FLT3 | acute myeloid leukemia | preclinical mouse model

Significance

Our work highlights the importance of investigating co-occurring driver mutations of a disease and provides a mouse model in which *Idh1* mutation, in the presence of mutant *Npm1c*, is linked to the development of overt AML. Our mutant strains may facilitate the generation of subtype-specific treatments for human AML and the dissection of mechanisms of disease progression, immune modulation, and drug treatment response and resistance.

Mutations in isocitrate dehydrogenase-1 and -2 (*IDH1* and *IDH2*) are observed in ~20% of human acute myeloid leukemia (AML) cases, with about half exhibiting *IDH1* mutations (usually *IDH1*^{R132}) and the other half possessing *IDH2* mutations (predominantly *IDH2*^{R140} or *IDH2*^{R172}) (1–6). Wild type (WT) IDH1/2 enzymes convert isocitrate to α-ketoglutarate (α-KG) (7), whereas mutant IDH1/2 acquire aberrant enzymatic activity that converts α-KG to D-2-hydroxyglutarate (D-2HG). D-2HG competitively inhibits α-KG-dependent enzymes such as Ten-eleven-translocation 2 (TET2) and Jumonji-C domain histone demethylases, resulting in altered DNA/histone methylation and impaired hematopoietic cell differentiation (3, 8, 9). Mutations in *TET2* are also found in 10 to 20% of AML patients, and are mutually exclusive with *IDH1/2* mutations (1, 2, 5, 6). Clinical use of inhibitors targeting mutant IDH1/2 can reverse the differentiation arrest of AML cells and induce hematologic responses in patients, although resistance via various mechanisms can happen (10–19).

In human AML, mutations in *IDH1/2* or *TET2* are rarely found in isolation, suggesting that other driver mutations cooperate to induce AML (1, 2, 5, 6). Indeed, mice harboring either a single *Idh1* or *Idh2* mutation generally develop chronic myeloproliferative disease but not overt AML (11, 20, 21). Among mice carrying solely a *Tet2* mutation, only a few develop AML, and then only late in life (22). In AML patients, *IDH1*^{R132} or *IDH2*^{R140} mutations occur most frequently alongside *NPM1* mutations, and less commonly with *FLT3* mutations. *NPM1c* (NPM1-cytoplasmic) mutations are small insertions that cause cytoplasmic retention of the protein (23); these occur in ~30% of AML patients (1, 2, 4–6). AML patients bearing *NPM1*c plus *IDH1/2* mutation (but not a *FLT3* mutation) have a relatively favorable clinical outcome following standard induction chemotherapy (1). On the other hand, *FLT3* is mutated in ~30% of AML cases, with internal tandem duplications (ITD) occurring most frequently (1, 2, 4–6); the presence of a *FLT3*^{ITD} is associated with an unfavorable clinical outcome (1, 24, 25).

Conditional knock-in mice harboring a humanized *Npm1*c allele show enhanced hematopoietic stem/progenitor cell self-renewal and expanded myelopoiesis, with only a few animals developing delayed onset AML (26). Similarly, *Flt3*^{ITD} murine models display

Reviewers: J.D., Washington University School of Medicine; and C.T.J., University of Colorado Denver.

Competing interest statement: R.L.L. is on the supervisory board of Qiagen and is a scientific advisor to Imago, Mission Bio, Syndax, Zentalis, Ajax, Bakx, Auron, Prelude, C4 Therapeutics and Isoplexis, for which he receives equity support. R.L.L. has consulted for Incyte, Janssen, Morphosys and Novartis. C.E.M. is a consultant at Tempus Labs and Co-Founder of Onegevity Health. T.W.M. is a consultant for AstraZeneca and Tessa Therapeutics. R.L.L. is on the supervisory board of Qiagen and is a scientific advisor to Imago, Mission Bio, Syndax, Zentalis, Ajax, Bakx, Auron, Prelude, C4 Therapeutics and Isoplexis, for which he receives equity support. T.W.M. owns equity in Treadwell Therapeutics Inc. and Agios Pharmaceuticals. R.L.L. has received honoraria from Astra Zeneca and Kura for invited lectures and from Gilead for grant reviews.

[1]T.S., J.L., and X.Z. contributed equally to this work.

[2]C.M. and J. Foox contributed equally to this work.

[3]To whom correspondence may be addressed. Email: tak.mak@uhn.ca.

This article contains supporting information online at https://www.pnas.org/lookup/suppl/doi:10.1073/pnas.2415779122/-/DCSupplemental.

Published May 16, 2025.

enhanced myelopoiesis but not AML, suggesting that malignant transformation requires more than one genetic lesion (27). Notably, when mice bearing mutant *Npm1c* are crossed with *Flt3*^{ITD} mice, AML develops within a few months (28, 29). Conditional *Idh2*^{R140} knock-in mice, as well as *Tet2* knock-out mice bearing *Flt3*^{ITD}, show an increased incidence of AML and have been used to test various combination targeted therapies (11, 30). However, there have been no reports to date on the phenotypes of mice harboring *Npm1c* combined with mutated *Idh1*.

Depending on the specific co-occurring mutation(s), *IDH1/2* mutations are likely to have dramatic, but potentially differing effects on a cell's epigenetics, transcriptome, and metabolism (31). Indeed, the clinical use of IDH1/2-targeted therapies has yielded a range of responses that vary among AML patients, with some *IDH1/2*-mutated cases not achieving remission (16, 17, 32, 33). It follows that, from a treatment perspective, it is important to elucidate the effects of co-occurring mutations to provide therapeutic alternatives for those who will not benefit from a particular IDH1/2-targeting regimen.

To investigate the leukemogenic cooperativity of *IDH1*^{R132} mutation with *FLT3*^{ITD} or *NPM1c* driver mutations, we generated and molecularly characterized single and double knock-in mouse models. Herein, we describe crucial differences in the phenotypic, transcriptomic, and epigenetic features of cells from these mutant animals, and explore the implications of these differences for leukemia treatment.

Results

Differing Gross Hematopoietic Phenotypes and Survival of *Idh1*^{R132};*Npm1c* vs. *Idh1*^{R132};*Flt3*^{ITD} Mice. To study whether the *IDH1*^{R132} mutation cooperates with either *NPM1c* or *FLT3*^{ITD} in the development of AML, we used *Vav-Cre* to generate two strains of conditional double knock-in mutant mice: *Vav-Cre;Idh1*^{R132H} plus the *Npm1c* mutation (denoted hereafter as *Idh1*^{R132};*Npm1c*), and *Vav-Cre;Idh1*^{R132H} plus the *Flt3*^{ITD} mutation (denoted as *Idh1*^{R132};*Flt3*^{ITD}). While *Idh1*^{R132} single mutant (*Vav-Cre;Idh1*^{R132H}, denoted as *Idh1*^{R132}) mice showed a survival curve similar to that of their *Vav-Cre* littermates (denoted as wild type; WT), the median survival of *Idh1*^{R132};*Npm1c* mice (253.5 d) was significantly shorter than that of *Npm1c* single mutant mice (*Vav-Cre;Npm1c*, denoted as *Npm1c;* 307.5 d) (P = 0.0165) (Fig. 1*A*). However, there was no difference in the survival of *Flt3*^{ITD} single mutants (*Vav-Cre;Flt3*^{ITD}, denoted as *Flt3*^{ITD}) vs. *Idh1*^{R132};*Flt3*^{ITD} double mutant animals (Fig. 1*A*). Guided by these survival differences, we chose to analyze our mutant mice at two time points: at a young age (5 to 7 mo for all strains) and when older (7 to 13 mo for *Npm1c* and *Idh1*^{R132};*Npm1c* mice, and 11 to 18 mo for *Flt3*^{ITD} and *Idh1*^{R132};*Flt3*^{ITD} mice).

Peripheral blood (PB) levels of D-2HG were comparably elevated in all young mice expressing *Idh1*^{R132}, regardless of the presence of *Npm1c* or *Flt3*^{ITD} (*SI Appendix*, Fig. S1*A*). In addition, all young mutant mice had enlarged spleens compared to WT controls (*SI Appendix*, Fig. S1*B*). CBC analysis revealed that young *Npm1c*, *Idh1*^{R132};*Npm1c, Flt3*^{ITD}, and *Idh1*^{R132};*Flt3*^{ITD} mice all exhibited anemia and thrombocytopenia, with marked thrombocytopenia being present in *Npm1c* and *Idh1*^{R132};*Npm1c* mice from the earliest times assessed (*SI Appendix*, Fig. S1 *C* and *D*). Young *Flt3*^{ITD} and *Idh1*^{R132};*Flt3*^{ITD} mice also showed elevated white blood cell (WBC) counts, with myeloid lineage skewing (*SI Appendix*, Fig. S1 *E–G*). Examination of older *Npm1c*, *Idh1*^{R132};*Npm1c*, *Flt3*^{ITD}, and *Idh1*^{R132};*Flt3*^{ITD} mice revealed splenomegaly, elevated WBC (with increased CD11b$^+$ myeloid lineage cells), anemia, and thrombocytopenia, with anemia being most severe in both double mutants (Fig. 1 *B–D* and *SI Appendix*, Fig. S1 *H–J*).

Histological analyses of BM from older *Npm1c*, *Idh1*^{R132};*Npm1c*, *Flt3*^{ITD}, and *Idh1*^{R132};*Flt3*^{ITD} mice revealed increased myeloid lineage cells and decreased megakaryocytes and erythroid cells (Fig. 1*E*). Morphologically immature blast cells were increased in number in the BM and PB of *Idh1*^{R132};*Npm1c* mice (Fig. 1 *E* and *F*). The degree of destruction of splenic architecture was similar for *Npm1c*, *Idh1*^{R132};*Npm1c, Flt3*^{ITD}, and *Idh1*^{R132};*Flt3*^{ITD} mice, as was cellular infiltration around blood vessels of the liver (*SI Appendix*, Fig. S1 *K* and *L*). The cells infiltrating livers were positive for MPO, indicating myeloid lineage commitment (*SI Appendix*, Fig. S1*L*). Flow cytometric analysis (FCA) confirmed these data, showing an increase in CD11b$^+$ myeloid cells, but a decrease in Ter119$^+$ erythroid progenitors in *Npm1c*, *Idh1*^{R132};*Npm1c*, and *Idh1*^{R132};*Flt3*^{ITD} BM (Fig. 1 *G* and *H* and *SI Appendix*, Fig. S1 *M* and *N*). There was also an increased proportion of CD11b$^+$ myeloid cells in the enlarged spleens of these animals (*SI Appendix*, Fig. S1*O*). CD11b$^+$ cells in *Idh1*^{R132};*Npm1c* mice showed only faint Gr1 expression, in keeping with their less mature phenotype (Fig. 1 *G* and *H* and *SI Appendix*, Fig. S1 *O* and *P*). Thus, although both *Idh1*^{R132};*Npm1c* and *Idh1*^{R132};*Flt3*^{ITD} mice develop myeloid disease, *Idh1*^{R132}-*Npm1c* cooperation has a more striking effect on myeloid cell differentiation and survival than does *Idh1*^{R132}-*Flt3*^{ITD} cooperation.

Distinct Hematopoietic Stem/Progenitor Phenotypes in *Idh1*^{R132};*Npm1c* vs. *Idh1*^{R132};*Flt3*^{ITD} Mutants. Young *Npm1c, Flt3*^{ITD}, *Idh1*^{R132};*Npm1c* and *Idh1*^{R132};*Flt3*^{ITD} mice all showed a significant decrease in lineage-negative (Lin$^-$) BM cells (stem and progenitor-enriched population), but only *Npm1c* and *Idh1*^{R132};*Npm1c* mice continued to do so as they aged (Fig. 2 *A* and *B* and *SI Appendix*, Fig. S2*A*). Regarding the composition of the Lin$^-$ cell compartment, the Lin$^-$IL-7R$^-$Sca1$^-$cKit$^+$ (LK) population, which contains common myeloid progenitors (CMPs), granulocyte macrophage progenitors (GMPs), and megakaryocyte erythrocyte progenitors (MEPs), was unchanged in terms of percentage and composition in both young and older *Npm1c* and *Idh1*^{R132};*Npm1c* mice (Fig. 2 *C–E* and *SI Appendix*, Fig. S2*B*). However, the percentage of Lin$^-$IL-7R$^-$Sca1$^+$cKit$^+$ (LSK) cells, which include hematopoietic stem cells (HSC) and multipotent progenitors, was decreased in older *Idh1*^{R132};*Npm1c* mice (Fig. 2 *F* and *G*). In contrast, while the percentage of LSK cells among Lin$^-$ cells was unchanged in older *Flt3*^{ITD} mice, the LK and LSK compartments were increased in both young and older *Idh1*^{R132};*Flt3*^{ITD} mice and in young *Flt3*^{ITD} mice (Fig. 2 *C, D, F,* and *G* and *SI Appendix*, Fig. S2*A*). The composition of the LK compartment was skewed toward GMP (FcγR$^+$CD34$^+$) at the expense of CMP (FcγR$^-$CD34$^+$) and MEP (FcγR$^-$CD34$^-$) (Fig. 2*E* and *SI Appendix*, Fig. S2*B*). In terms of the LSK population composition, we observed a significant decrease in long-term (LT)-HSC (CD150$^+$CD48$^-$) in young *Npm1c* and *Idh1*^{R132};*Npm1c* mice (Fig. 2*H* and *SI Appendix*, Fig. S2*C*). The same trend was even more marked in young *Flt3*^{ITD} and *Idh1*^{R132};*Flt3*^{ITD} mice (Fig. 2*H* and *SI Appendix*, Fig. S2*C*).

The total cKit$^+$ population, which normally includes hematopoietic stem and progenitor cells, was expanded in all *Npm1c*, *Flt3*^{ITD}, *Idh1*^{R132};*Npm1c*, and *Idh1*^{R132};*Flt3*^{ITD} mice but with important differences (Fig. 2 *I–K*). Intriguingly, regardless of age, the expanded cKit$^+$ cells in *Npm1c* and *Idh1*^{R132};*Npm1c* mice coexpressed CD11b, whereas the expanded cKit$^+$ cells in *Flt3*^{ITD} and *Idh1*^{R132};*Flt3*^{ITD} mice were CD11b$^-$ (Fig. 2 *I–K*). In addition, some CD11b$^+$ cells in

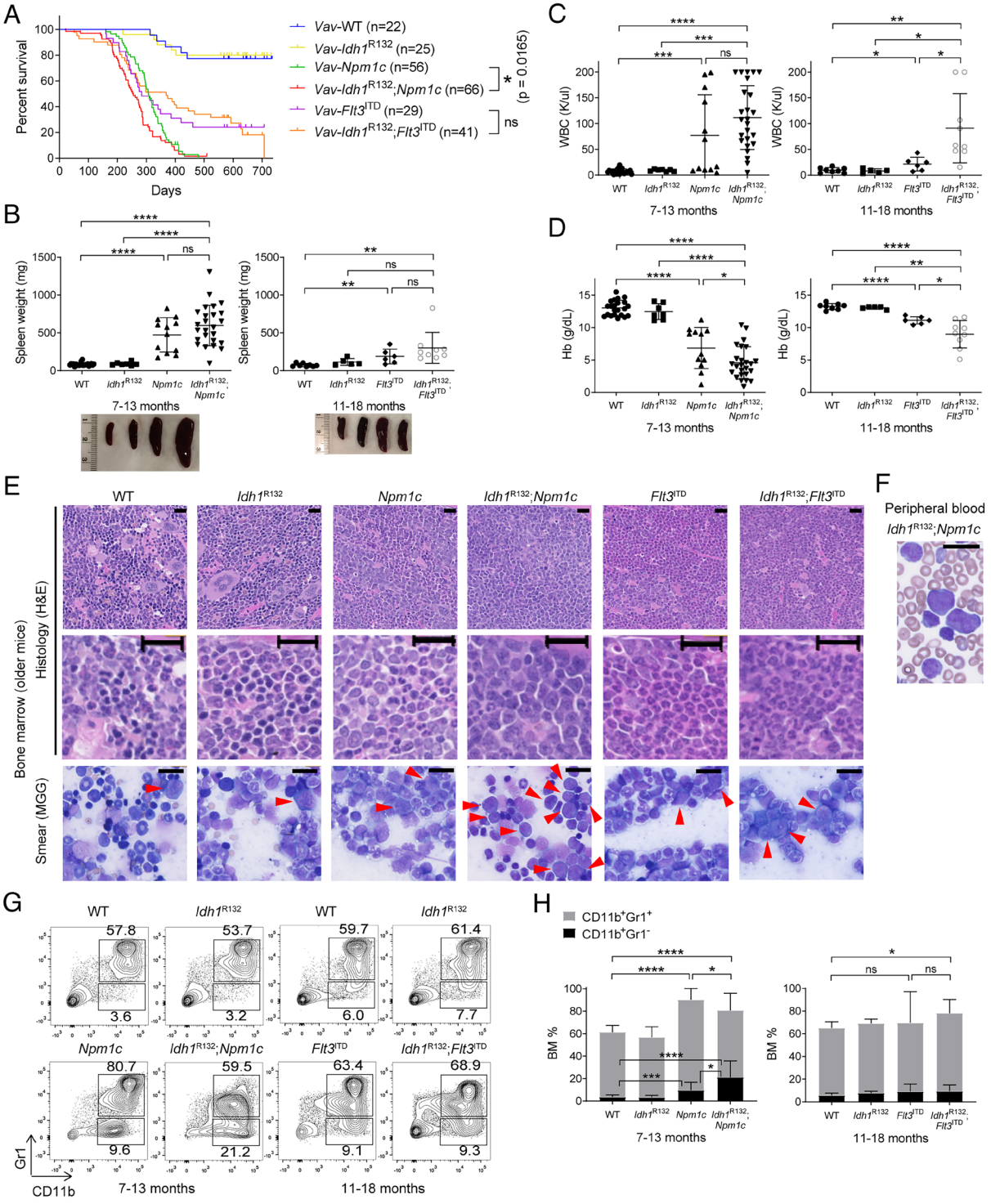

Fig. 1. Differing gross hematopoietic phenotypes of *Idh1*^{R132};*Npm1c* vs. *Idh1*^{R132};*Flt3*^{ITD} mice. (*A*) Kaplan–Meier survival curves of WT, *Idh1*^{R132}, *Npm1c*, *Idh1*^{R132};*Npm1c*, *Flt3*^{ITD}, and *Idh1*^{R132};*Flt3*^{ITD} mice. For survival curves in all Figures, *P* values were calculated by the log-rank test. **P* < 0.05, ***P* < 0.01 and ****P* < 0.001. ns, not significant. (*B*, *Top*) Quantitation of weights of spleens from 7 to 13 mo old WT (n = 23), *Idh1*^{R132} (n = 7), *Npm1c* (n = 12), and *Idh1*^{R132};*Npm1c* (n = 25) mice, and from 11 to 18 mo old WT (n = 8), *Idh1*^{R132} (n = 5), *Flt3*^{ITD} (n = 6), and *Idh1*^{R132};*Flt3*^{ITD} (n = 9) mice. (*Bottom*) Representative macroscopic images of spleens from the mice in the *Top* panels. For all panels of this type, values represent individual mice, with the mean ± SD also shown. For all Figures, unless otherwise indicated, data are the mean ± SD, with **P* < 0.05, ***P* < 0.01, ****P* < 0.001 and *****P* < 0.0001 as assessed by unpaired Student's *t* test. (*C* and *D*) White blood cell (WBC) counts (*C*) and hemoglobin (Hb) levels (*D*) in 7 to 13 mo old cohorts of WT (n = 22), *Idh1*^{R132} (n = 7), *Npm1c* (n = 12), and *Idh1*^{R132};*Npm1c* (n = 25) mice, and in 11 to 18 mo old cohorts of WT (n = 8), *Idh1*^{R132} (n = 5), *Flt3*^{ITD} (n = 6), and *Idh1*^{R132};*Flt3*^{ITD} (n = 9) mice. (*E*) Representative images of H&E-stained bone marrow (BM) sections at two magnifications (*Top* and *Middle*), and May-Gründwald-Giemsa (MGG)-stained BM smears (*Bottom*), from aged mice of the indicated genotypes. Red arrowheads indicate blasts. (Scale bars, 20 μm.) (*F*) Representative image of an MGG-stained peripheral blood (PB) smear from an aged *Idh1*^{R132};*Npm1c* mouse with leukemic disease. (Scale bar, 20 μm.) (*G*) Representative flow cytometric analyses of CD11b and Gr1 expression among viable BM cells from (*Left*) 7 to 13 mo old WT (n = 22), *Idh1*^{R132} (n = 7), *Npm1c* (n = 12), and *Idh1*^{R132};*Npm1c* (n = 23) mice, and (*Right*) 11 to 18 mo old WT (n = 8), *Idh1*^{R132} (n = 5), *Flt3*^{ITD} (n = 6), and *Idh1*^{R132};*Flt3*^{ITD} (n = 9) mice. For all flow cytometric data, numbers in specific compartments are the mean percentage. (*H*) Quantitation of frequencies of CD11b^{+}Gr1^{+} and CD11b^{+}Gr1^{-} cells from the data in (*G*).

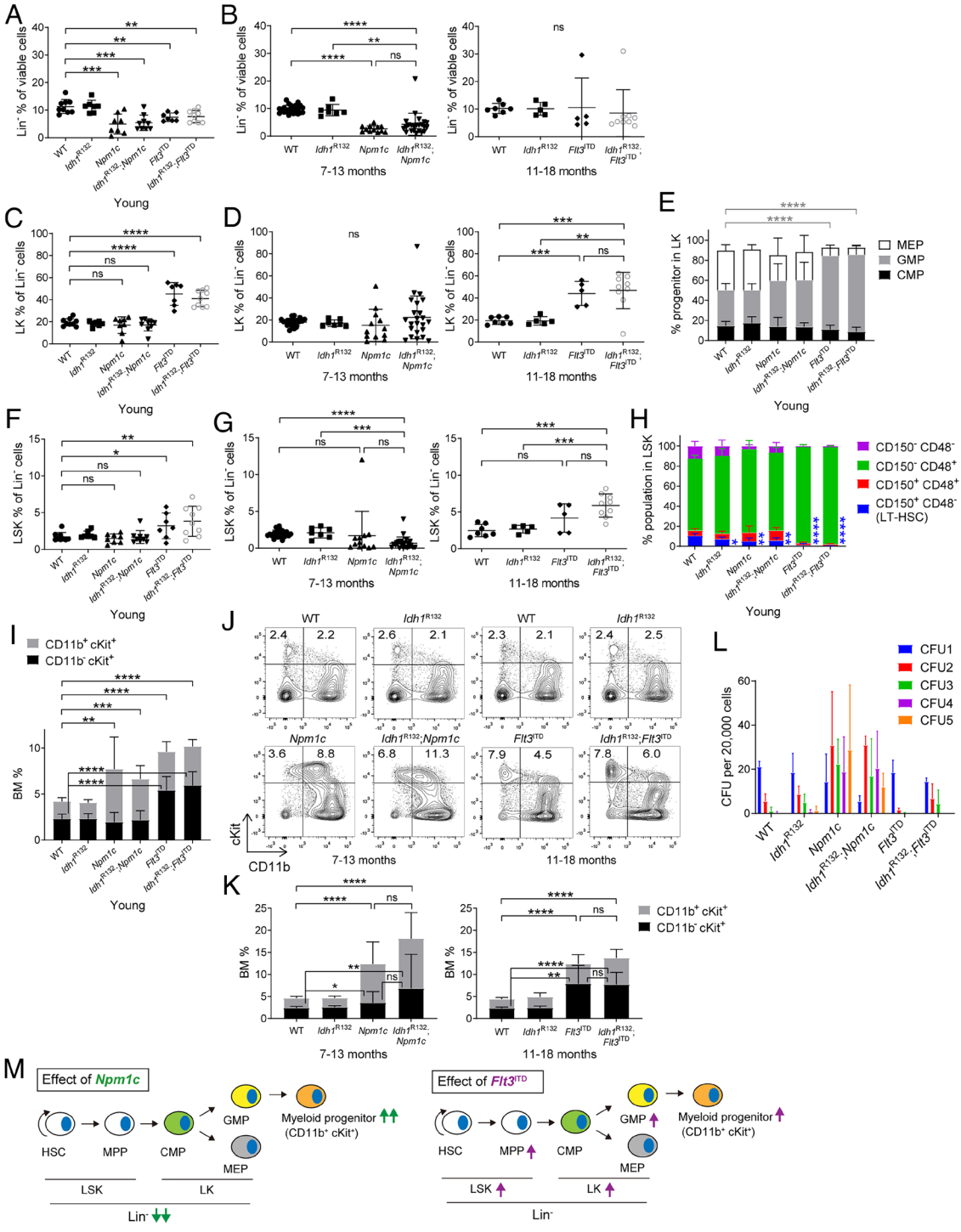

Fig. 2. Distinct stem/progenitor cell phenotypes exhibited by *Idh1*^{R132};*Npm1c* vs. *Idh1*^{R132};*Flt3*^{ITD} mutants. (*A*) Frequency of cells negative for any lineage-differentiated cell surface marker (Lin$^-$ cells) among viable total BM cells from young mice of the indicated genotypes (n = 7 to 9/group). See also *SI Appendix*, Fig. S2*A*. (*B*) Frequency of Lin$^-$ cells among viable total BM cells from (*Left*) 7 to 13 mo old WT (n = 23), *Idh1*^{R132} (n = 7), *Npm1c* (n = 12), and *Idh1*^{R132};*Npm1c* (n = 23) mice, and from (*Right*) 11 to 18 mo old WT (n = 7), *Idh1*^{R132} (n = 5), *Flt3*^{ITD} (n = 5), and *Idh1*^{R132};*Flt3*^{ITD} (n = 9) mice. (*C*) Frequency of LK (Lin$^-$IL-7R$^-$Sca1$^-$cKit$^+$) cells among the Lin$^-$ BM cells isolated from the young mice in *A*. See also *SI Appendix*, Fig. S2*A*. (*D*) Frequencies of LK cells among the Lin$^-$ BM cells isolated from the aged mice in *B*. (*E*) Frequencies of CMP (FcγR$^-$CD34$^+$), GMP (FcγR$^+$CD34$^+$), and MEP (FcγR$^-$CD34$^-$) progenitors in the LK fraction from young mice of the indicated genotypes (n = 6 to 10/group). See also *SI Appendix*, Fig. S2*B*. (*F*) Frequency of LSK (Lin$^-$IL-7R$^-$Sca1$^+$cKit$^+$) cells among the Lin$^-$ BM cells isolated from the young mice in *A*. See also *SI Appendix*, Fig. S2*A*. (*G*) Frequencies of LSK cells among the Lin$^-$ BM cells isolated from the aged mice in *B*. (*H*) Frequencies of CD150$^+$CD48$^-$ (LT-HSC) cells and the other indicated cell populations within LSK fractions isolated from young mice of the indicated genotypes (n = 4 to 9/group). See also *SI Appendix*, Fig. S2*C*. (*I*) Frequencies of CD11b$^-$cKit$^+$ cells and CD11b$^+$cKit$^+$ cells among viable BM cells from young mice of the indicated genotypes (n = 7 to 10/group). (*J*) Representative FCA of cKit and CD11b expression among viable total BM cells from (*Left*) 7 to 13 mo old WT (n = 23), *Idh1*^{R132} (n = 7), *Npm1c* (n = 12), and *Idh1*^{R132};*Npm1c* (n = 23) mice, and (*Right*) 11 to 18 mo old WT (n = 8), *Idh1*^{R132} (n = 5), *Flt3*^{ITD} (n = 6), and *Idh1*^{R132};*Flt3*^{ITD} (n = 9) mice. (*K*) Frequencies of CD11b$^-$cKit$^+$ and CD11b$^+$cKit$^+$ cells among the cells in *J*. (*L*) Colony formation assays of BM cells that were isolated from young mice of the indicated genotypes and serially plated five times in methylcellulose medium (CFU 1-5) (n = 3). (*M*) Schematic diagram summarizing the differing effects of the *Npm1c* and *Flt3*^{ITD} mutations on hematopoietic cell differentiation toward the myeloid lineage.

Npm1c and *Idh1*^{R132};*Npm1c* mice expressed the B cell marker B220^{+} but not CD19, a second B cell marker (*SI Appendix*, Fig. S2 *D–H*). These data suggest that aberrant coexpression of B220 and CD11b on myeloid lineage cells emerges as disease develops in *Npm1c* and *Idh1*^{R132};*Npm1c* mice, as previously observed in other mouse AML models (34, 35).

To assess the self-renewal potential of mutant BM cells, we performed colony formation assays and serial replating experiments in methylcellulose. BM cells from WT and *Flt3*^{ITD} mice did not form colonies after two rounds of replating (Fig. 2*L*). *Idh1*^{R132} and *Idh1*^{R132};*Flt3*^{ITD} BM cells formed colonies in a third plating but not thereafter, demonstrating that the *Idh1*^{R132} mutation increases in vitro self-renewal potential to a moderate extent. In marked contrast, *Npm1c* and *Idh1*^{R132};*Npm1c* BM cells generated large numbers of colonies upon initial plating and four rounds of replating. Considering the continued robust replating, no further passages were performed. Of note, there was no significant difference between the replating of cells from *Npm1c* and *Idh1*^{R132};*Npm1c* mice, suggesting that the *Npm1c* mutation alone was responsible for the dramatic impact on self-renewal potential. Such an effect is to be expected based upon the effect of *Npm1c* on HoxA9 and HoxA10 expression (36, 37). Thus, mice bearing an *Idh1*^{R132} mutation showed distinct hematopoietic stem/progenitor immunophenotypes according to whether the *Idh1*^{R132} was coexpressed with mutant *Npm1c* or *Flt3*^{ITD} (Fig. 2*M*).

***Idh1*^{R132};*Npm1c* and *Idh1*^{R132};*Flt3*^{ITD} cKit^{+} Cells Show Distinct Transcriptomic Signatures.** To investigate these phenotypic differences at the molecular level, we isolated cKit^{+} cells from 3- and 6-mo-old WT and mutant mice and performed RNA sequencing (RNA-seq). Principal Component Analysis (PCA) indicated that these samples segregated based on the presence of *Flt3*^{ITD} or *Npm1c* and not *Idh1*^{R132}, as *Idh1*^{R132};*Npm1c* and *Idh1*^{R132};*Flt3*^{ITD} samples displayed distinct gene expression profiles (*SI Appendix*, Fig. S3*A*). By Gene Set Enrichment Analysis (GSEA), the top upregulated pathways in *Idh1*^{R132};*Npm1c* cKit^{+} cells (compared to WT) included gene sets related to the immune system, especially interferon α/γ responses (Fig. 3*A*). Downregulated pathways in *Idh1*^{R132};*Npm1c* cells included gene sets related to oxidative phosphorylation (OXPHOS) and respiratory electron transport chain (ETC) (Fig. 3*A*). For the mice with *Flt3*^{ITD} mutation, with or without *Idh1*^{R132}, we observed changes similar to those previously reported for *Flt3*^{ITD} mouse models (*SI Appendix*, Fig. S3*B*) (30, 38). Of interest, genes related to heme metabolism and transporter activity were downregulated, as were genes regulated by the erythroid-enriched transcription factor KLF1 (Fig. 3*A*) (39). To identify which pathways were affected by *Idh1*^{R132} mutation, we applied comparative GSEA to *Idh1*^{R132};*Npm1c* vs. *Npm1c* cells. Once again, we detected enrichment of genes related to the immune system and interferon responses in the double mutant cells as compared to the single mutant cells. We also observed decreases in the expression of genes related to heme metabolism, transporter activity, and KLF1 target genes (Fig. 3*A*).

To extend our examinations beyond gene sets, we compared the expression levels of individual genes. The use of Venn diagrams to compare levels in single and double mutant cells from young or older mice revealed that the altered gene expression patterns were more reflective of the effects of *Npm1c* or *Flt3*^{ITD} than of *Idh1*^{R132} (Fig. 3*B*). Of note, the majority of differentially expressed genes (DEGs) in *Idh1*^{R132};*Npm1c* double mutant cells differed from those in *Npm1c* and *Idh1*^{R132} single mutant cells. In contrast, most DEGs in *Idh1*^{R132};*Flt3*^{ITD} cells overlapped with those in *Flt3*^{ITD} cells (Fig. 3*B* and *SI Appendix*, Table S1). A key feature of *Npm1c*-related disease was the variable but increased expression of Hox gene family members, regardless of the presence of mutant *Idh1*^{R132} (Fig. 3*B* and *SI Appendix*, Fig. S3*C*) (26, 40). Comparison of *Idh1*^{R132};*Npm1c* vs. *Npm1c* cells revealed 10 upregulated genes in the double mutant cells, including immune system genes (*Wdfy1*, *Itga1*, *Tlr1*), and 21 downregulated genes, including a transporter gene (*Fabp4*) and KLF1 target genes (*Fabp4*, *Tspan9*) (Fig. 3*B* and *SI Appendix*, Fig. S3*C* and Tables S1 and S2). Regarding mice with *Flt3*^{ITD} mutation, there was increased expression of *Il2ra*, *Socs2*, *Socs2-AS1,* and the pSTAT5 target *Cish* (41–43); again, these alterations were not affected by mutant *Idh1*^{R132} (Fig. 3*B* and *SI Appendix*, Fig. S3*C* and Table S1). Intriguingly, direct comparison of *Idh1*^{R132};*Flt3*^{ITD} vs. *Flt3*^{ITD} cells revealed the differential expression of only one gene, namely *Ppbp* (*SI Appendix*, Fig. S3*C* and Tables S1). Both *Flt3*^{ITD} and *Idh1*^{R132};*Flt3*^{ITD} cells showed a reduction in *Gata1,* in keeping with the development of anemia in *Flt3*^{ITD}-bearing mice. As well, there was a trend toward decreased *Gata1* levels in *Npm1c* and *Idh1*^{R132};*Npm1c* cells isolated from older mice, but this reduction was not statistically significant. The presence of *Idh1*^{R132} mutation had no effect on *Gata1* expression levels (Fig. 3*B* and *SI Appendix*, Fig. S3*C*).

In summary, *Idh1*^{R132};*Npm1c* and *Idh1*^{R132};*Flt3*^{ITD} cKit^{+} cells showed distinct transcriptomic signatures, with more dramatic effects being demonstrated when the *Idh1*^{R132} mutation was coupled with *Npm1c*.

***Idh1*^{R132} Cooperates with *Npm1c* to Induce AML in Mice.** When we assessed the nature of the diseases present in moribund animals using histological and flow cytometric analyses, we found that most of the diseases arising in *Npm1c* and *Idh1*^{R132};*Npm1c* animals were myeloid neoplasms. Regarding *Idh1*^{R132};*Flt3*^{ITD} mice, ~25% of animals developed a T cell proliferation, while the rest exhibited myeloid neoplasms. For a myeloid neoplasm to be defined as AML in a mouse model, according to the Bethesda proposed criteria, the immature blast cells in question must cause lethality within 8 wk after transplantation into recipient mice (44). To test our mutant cells for this capacity, we transplanted BM cells from moribund mice into CD45.1^{+} WT recipients: 31 *Idh1*^{R132};*Npm1c,* 9 *Npm1c*, and 7 *Idh1*^{R132};*Flt3*^{ITD} (Fig. 4*A*). Cells from 14/31 moribund *Idh1*^{R132};*Npm1c* mice resulted in the death of the recipients within 8 wk, while all but three recipients transplanted with cells from the other 17/31 mice all died by 150 d. At the time of death, the bone marrow and spleens of all *Idh1*^{R132};*Npm1c* secondary recipients consisted of predominantly myelo-monocytic blast cells (*SI Appendix*, Fig. S4 *A–G*). In addition, the transplanted cells from *Idh1*^{R132};*Npm1c* transplanted animals that died before 8 wk could be serially transplanted multiple times, consistently generating AML in the recipient mice (*SI Appendix*, Fig. S4*H*). In contrast, recipients from 1/9 moribund *Npm1c* and 1/7 moribund *Idh1*^{R132};*Flt3*^{ITD} mice died within 8 wk. Moreover, for the majority of moribund *Npm1c* and *Idh1*^{R132};*Flt3*^{ITD} mice, the recipient animals were still alive at day 150 (Fig. 4 *A* and *B*). Thus, only the combination of *Idh1*^{R132} plus *Npm1c* induced AML in mice with a high incidence.

To determine whether *Idh1*^{R132};*Npm1c* AML cells had acquired additional somatic mutations, we performed targeted sequencing of known cancer genes (Profiling of Actionable Cancer Targets; PACT sequencing) (45) on cells from 10 *Idh1*^{R132};*Npm1c* AML mice. The AML cells from one such animal had acquired mutations of *Nras* and *Pik3ca,* both at a variant allele frequency (VAF) of 0.44, indicative of their presence in almost all of the cells (Fig. 4*C* and *SI Appendix*, Table S3). Acquired mutations at a lower VAF (0.07 to 0.17) were found in cells from six other mice (Fig. 4*C*). While the combination of *Idh1*^{R132} plus *Npm1c* is

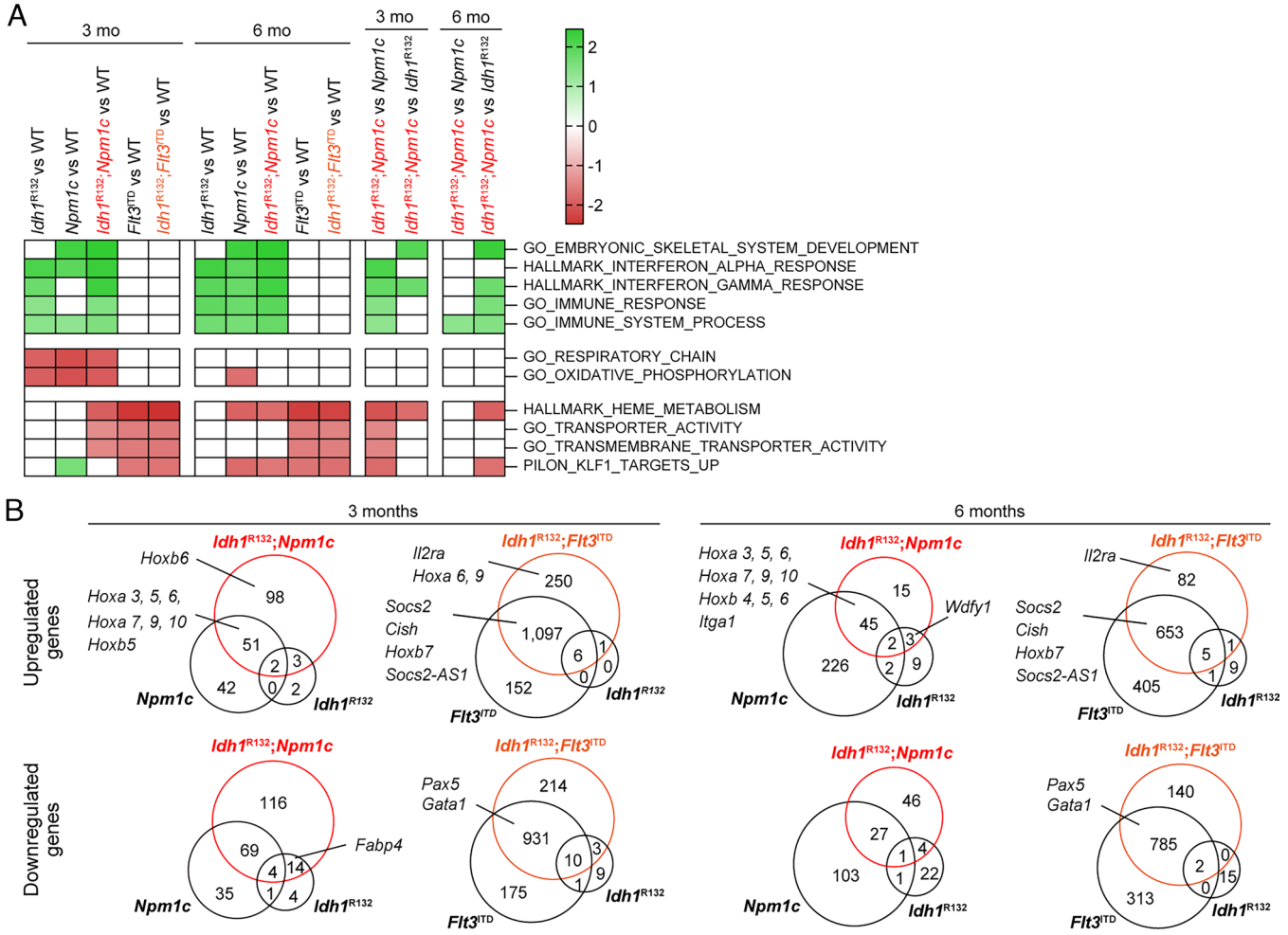

Fig. 3. Distinct transcriptomic signatures of *Idh1*^{R132};*Npm1c* vs. *Idh1*^{R132};*Flt3*^{ITD} cKit$^+$ cells. (*A*) GSEA of RNA-seq data of cKit$^+$ cells isolated from mice of the indicated genotypes at 3 or 6 mo of age. Significant enrichment (green) and significant depletion (red) are based on NES for the indicated comparison (q < 0.05). Blank columns, not significant. (*B*) Venn diagrams showing numbers of overlapping up- or down-regulated genes in cKit$^+$ cells from 3-mo-old (*Left*) and 6-mo-old (*Right*) mice of the indicated genotypes (compared to WT). Differential gene expression analysis was performed using DESeq2, and genes with fold-change >1.5 and adjusted *P*-value <0.01 were regarded as differentially expressed. Genes of interest are indicated.

sufficient to induce AML in mice, the acquisition of recurrent mutations of *Nras*, *Ptpn11,* and *Pik3ca* was in keeping with what is seen in human disease (46). It is possible that these spontaneous mutations in the RAS signaling pathway confer a growth advantage on *Idh1*^{R132};*Npm1c* AML cells.

The cell compartment containing leukemia-initiating cells (LICs) varies across mouse models, and may include GMP (40, 47), LSK (30, 40), or CD11b$^+$cKit$^+$ cells (48). Because our *Idh1*^{R132};*Npm1c* AML mice showed an increased proportion of cKit$^+$ cells, we sought to determine whether these cells had the properties of LICs. To this end, we transplanted cKit$^+$ cells from BM of *Idh1*^{R132};*Npm1c* AML mice into CD45.1$^+$ WT recipients and observed the induction of lethal AML (*SI Appendix*, Fig. S4 *I–L*). Interestingly, some recipients of cKit$^-$ *Idh1*^{R132};*Npm1c* AML BM cells also demonstrated engraftment and lethality (*SI Appendix*, Fig. S4 *I–L*); however, the cells from the AML developing in these mice were cKit$^+$. This result can be explained either by the presence of contaminating residual cKit$^+$ cells among the transplanted cKit$^-$ cells, or by an ability of cKit$^-$ cells to regain cKit expression. Regardless, these studies show that LICs are enriched in the cKit$^+$ compartment in *Idh1*^{R132};*Npm1c* AML mice.

Next, we sought to further define the cell compartment in which LICs were enriched by isolating the LSK, GMP, and CD11b$^+$cKit$^+$ cell fractions from BM of two *Idh1*^{R132};*Npm1c* AML mice (#5 and #10) and repeating the transplantation experiments. In both cases, transplanted mutant CD11b$^+$cKit$^+$ cells and LSK cells showed more aggressive expansion in recipients compared to GMP cells (*SI Appendix*, Fig. S4 *M* and *N*). While we observed variation in survival among the recipients of cell subsets from these two AML mouse lines, the CD11b$^+$cKit$^+$ cell compartment was consistently enriched with LICs compared to the other compartments (Fig. 4*D*).

To investigate the clinical relevance of our mouse model, we analyzed a published dataset of AML patient samples (6). DEG signatures similar to those of our mouse *Idh1*^{R132};*Npm1c* cKit$^+$ cells were observed for human AML cells bearing *NPM1* or *NPM1* plus *IDH1* mutations (Fig. 4*E*). GSEA indicated that gene sets related to transporter activity, heme metabolism, and KLF1 targets were downregulated in human AML cells bearing *NPM1* plus *IDH1* mutations compared to AML cells lacking a *FLT3*, *NPM1,* or *IDH1* mutation (Fig. 4*F*). Regarding individual loci, downregulation of genes related to transporter activity (*Slc2a4*, *Atp2c2*) and heme metabolism (*Gypa*) were found both in murine *Idh1*^{R132};*Npm1c* cells and in human *NPM1* plus *IDH1*-mutant AML cells (*SI Appendix*, Fig. S4*O*). Thus, our *Idh1*^{R132};*Npm1c* mouse model has a transcriptomic profile that recapitulates that of the corresponding human AML.

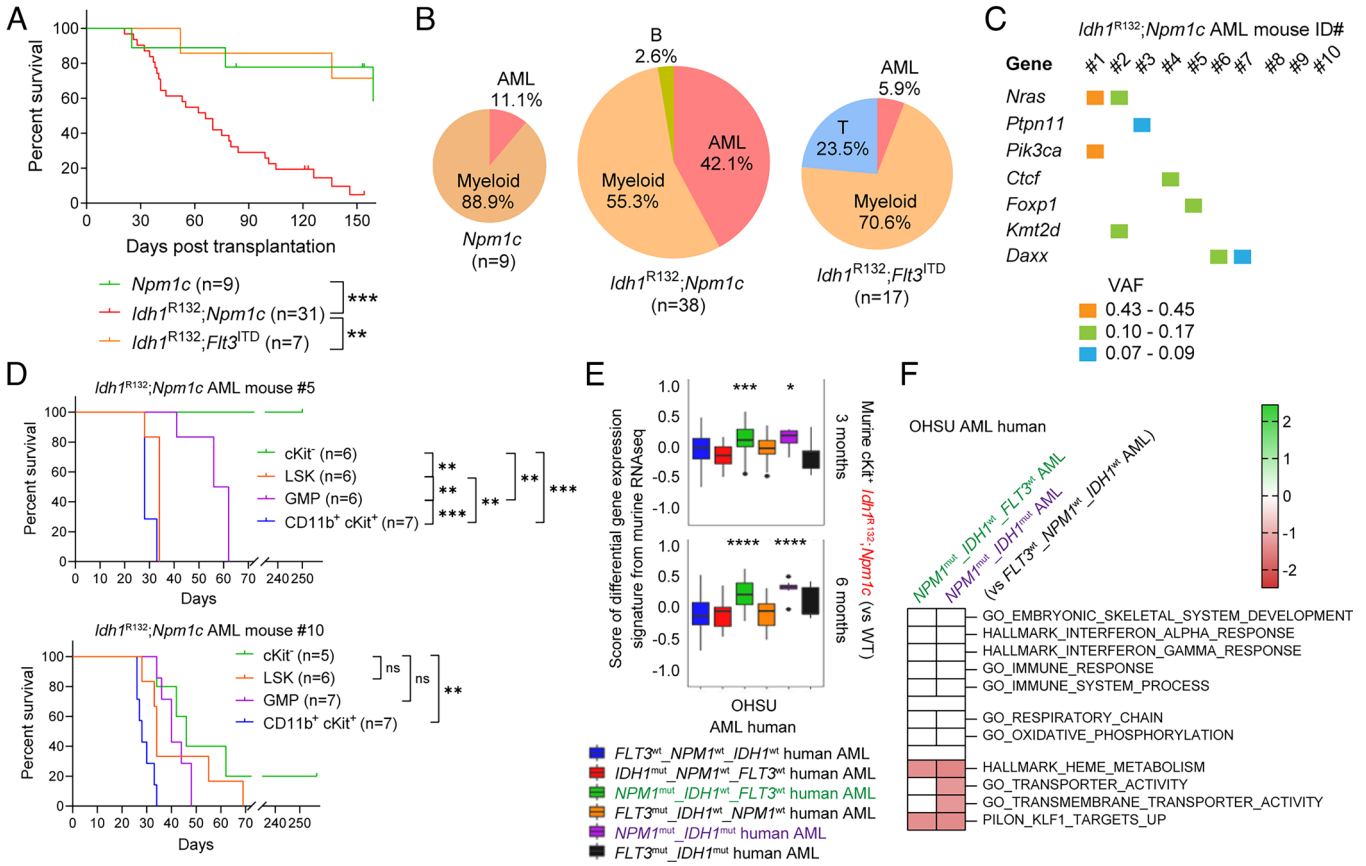

Fig. 4. *Idh1*^{R132} cooperates with *Npm1c* to induce AML in mice. (*A*) Kaplan–Meier survival curves of CD45.1^{+} recipient mice transplanted with BM cells from moribund mice of the indicated genotypes. (*B*) Pie charts depicting the relative frequencies of diseases developing in mice of the indicated genotypes. AML was deemed to be present if disease developed rapidly and was fatal to transplant recipients within 8 wk (red). "Myeloid" was defined as disease featuring myeloid cell proliferation but not judged to be AML (orange). "B" indicates a disease featuring B cell proliferation (green). "T" indicates a disease featuring T cell proliferation (blue). (*C*) Identification of the indicated somatic mutations in 10 lines of *Idh1*^{R132};*Npm1c* mice exhibiting AML. VAF, variant allele frequency, with three different ranges shown. (*D*) Kaplan–Meier survival curves of recipient mice transplanted with cKit^{-} cells, CD11b^{+}cKit^{+} cells, GMP, or LSK cells from *Idh1*^{R132};*Npm1c* AML mice. Two mouse lines of transplantable *Idh1*^{R132};*Npm1c* AML (#5, *Top*; #10, *Bottom*) were used. (*E*) Similarities in gene expression signatures between human primary AML cells bearing the indicated mutations and cKit^{+} cells from 3- or 6-mo-old *Idh1*^{R132};*Npm1c* mice. Shown are gene set variation analysis (GSVA) scores of human AML samples from a published Oregon Health & Science University (OHSU) cohort (Nature, 2018) as determined using the murine differential gene expression signature of *Idh1*^{R132};*Npm1c* vs. WT. Human samples are combinatorially partitioned by their *NPM1*, *IDH1*, and *FLT3* genotypes. (*F*) GSEA based on transcriptomic data from human AML samples (OHSU, Nature 2018) bearing the indicated gene mutations vs. human AML with no *FLT3*, *NPM1*, or *IDH1* mutations. Significant depletion (red) is based on NES for the indicated comparison (q < 0.05). Blank columns, not significant.

***Idh1*^{R132} has a Modest Effect on *Npm1c*-Induced Phenotypes through Epigenetic Modifications.** Given the known effects of *IDH* mutations on epigenetics (7–9), we subjected cKit^{+} cells from our mutant strains (at 6 mo of age) to chromatin accessibility profiling by "Assay for Transposase-Accessible Chromatin using sequencing" (ATAC-seq), as well as to DNA methylation profiling by bisulfite-sequencing. Overall, *Idh1*^{R132} alone induced only very weak changes to chromatin accessibility (*SI Appendix*, Fig. S5*A*). The *Npm1c* and *Idh1*^{R132};*Npm1c* mutations were associated with larger epigenetic changes, but very few were statistically significant due to variation among animals (*SI Appendix*, Fig. S5*A*). Compared to WT mice, changes observed in *Npm1c* cKit^{+} cells were predominantly "chromatin opening" loci, whereas *Idh1*^{R132};*Npm1c* cKit^{+} cells showed almost no significant chromatin accessibility changes (*SI Appendix*, Fig. S5*A*). cKit^{+} cells from *Flt3*^{ITD} mice and *Idh1*^{R132};*Flt3*^{ITD} mice showed less variation among animals, allowing for statistically significant conclusions to be drawn. Compared to WT cells, cKit^{+} cells from *Flt3*^{ITD} or *Idh1*^{R132};*Flt3*^{ITD} mice displayed many chromatin accessibility changes, most of which were "chromatin closing loci". *Idh1*^{R132};*Flt3*^{ITD} cKit^{+} cells displayed fewer opening chromatin peaks than *Flt3*^{ITD} cKit^{+} cells (*SI Appendix*, Fig. S5*A*). Thus, *Idh1*^{R132} appears to partially counteract *Npm1c*- or *Flt3*^{ITD}-driven chromatin opening. Of note, changes in chromatin accessibility near gene transcription start sites (TSS) correlated significantly with gene expression changes across all genotypes (*SI Appendix*, Fig. S5*B*). For instance, we found several opening chromatin loci in the *Hoxa* gene cluster in *Npm1c* cells, and opening peaks in the *Socs2* promoter in *Flt3*^{ITD} and *Idh1*^{R132};*Flt3*^{ITD} cells (*SI Appendix*, Fig. S5 *C* and *D*).

With respect to DNA methylation, *Idh1*^{R132} alone was associated with relatively modest changes compared to *Npm1c* or *Flt3*^{ITD} alone, but substantial alterations were evident when *Idh1*^{R132} was combined with *Npm1c* or *Flt3*^{ITD} (Fig. 5). Compared to *Npm1c* cells, *Idh1*^{R132};*Npm1c* cells showed fewer hypo- and hypermethylated loci, with the greatest difference being more hypomethylated sites in the *Npm1c* only cells. A similar but smaller effect was seen when comparing *Idh1*^{R132};*Flt3*^{ITD} and *Flt3*^{ITD} samples. Thus, in general, *Idh1*^{R132} appears to antagonize hypomethylation changes that occur in the presence of *Npm1c* and *Flt3*^{ITD}, while also driving gains of methylation at different loci. It follows that these DNA methylation modifications may influence the transcriptome. Indeed, the overall downregulated level of gene expression in *Idh1*^{R132};*Npm1c* cells correlated with hypermethylation in TSS-proximal regions (*SI Appendix*, Fig. S5*E*).

To better understand how the *Idh1*^{R132} mutation influenced *Npm1c* cells, we isolated BM cells from our *Npm1c* or *Idh1*^{R132};*Npm1c*

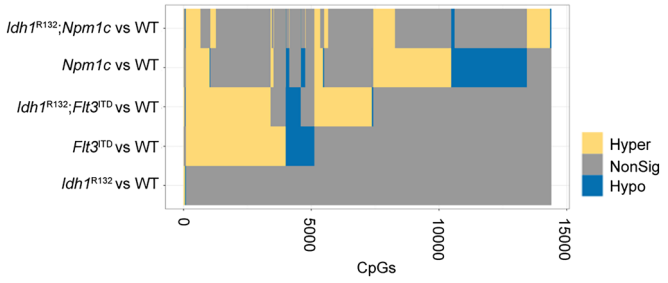

Fig. 5. *Idh1*^{R132} has a modest effect on *Npm1c*-induced phenotypes through epigenetic modifications. Plot depicting loci with hyper- or hypomethylated CpGs, as determined by bisulfite-sequencing, in cKit$^+$ cells from 6-mo-old mice of the indicated genotypes.

mice and established cell lines (18) (denoted as *OCI-Idh1*^{WT}*Npm1c_cells* and *OCI-Idh1*^{R132}*Npm1c_cells*, respectively) (*SI Appendix*, Fig. S6*A*). The double mutant cell line continued to produce D-2HG in vitro (*SI Appendix*, Fig. S6*B*). To characterize these cell lines at the molecular level, we performed RNA-seq analyses (18) and found that pathways related to cell movement and transporters were more enriched in *OCI-Idh1*^{WT}*Npm1c_cells* than in *OCI-Idh1*^{R132} *Npm1c_cells*. In contrast, pathways involving cell division and development were more enriched in *OCI-Idh1*^{R132}*Npm1c_cells* than in *OCI-Idh1*^{WT}*Npm1c_cells* (*SI Appendix*, Fig. S6*C* and Table S4). As shown in *SI Appendix*, Fig. S6*D*, *OCI-Idh1*^{R132}*Npm1c_cells* also displayed enrichment in pathways related to nucleic acid, miRNA, and ribonucleotide pathways as well as fructose and ribose phosphate metabolic processes, which are linked to nucleic acid synthesis (49). Notably, the double mutant cell line exhibited enrichment in pathways positively regulating cytokine production. Conversely, *OCI-Idh1*^{WT}*Npm1c_cells* showed enrichment in pathways associated with cell differentiation processes (*SI Appendix*, Fig. S6*D*).

Several of the above observations stemming from our mouse AML cell line work parallel the human situation. For example, in keeping with previous findings in patients with *IDH1*-mutated AML (50) and categories of AML differentiation-arrest based on cell surface protein expressions (51), our RNA-seq data showed that disease developing in *Idh1*^{R132};*Npm1c* mice was of a more immature phenotype based on the greater expression of CD117 (Kit) and MPO as compared to disease in *Npm1c* mice (*SI Appendix*, Fig. S6 *E* and *F*). The expression of MPO was confirmed by western blot (*SI Appendix*, Fig. S6*G*). Cultures of *OCI-Idh1*^{R132}*Npm1c_cells* also contained a higher percentage of CD11b$^+$ cKit$^+$ cells compared to *OCI-Idh1*^{WT}*Npm1c_cells* (*SI Appendix*, Fig. S6*H*). Finally, we demonstrated that *OCI-Idh1*^{R132}*Npm1c_cells* showed enhanced activation of p38 MAPK (*SI Appendix*, Fig. S6*G*), which functions in a cytokine signaling pathway promoting AML cell growth (52, 53).

Effects of Combined *Idh1*^{R132} and *Npm1c* Mutations on Responses to Chemotherapy and IDH Inhibitor Treatments. Cases of cytogenetically defined intermediate-risk human AML bearing *NPM1* plus *IDH1/2* mutations have a more favorable clinical outcome than AML patients with *FLT3*^{ITD}, following treatment (*SI Appendix*, Fig. S7*A*) (1, 6, 24, 25). Standard treatment (with curative intent) for AML patients is cytotoxic chemotherapy using a combination of an anthracycline plus cytarabine (Ara-C). We hypothesized that the more favorable outcome for AML patients with *NPM1* plus *IDH1/2* mutations might be linked to a greater sensitivity to chemotherapy. To test this hypothesis, we carried out in vitro colony formation assays of drug-treated WT and mutant mouse cells. We observed that BM cells from *Idh1*^{R132};*Npm1c* mice were more sensitive to daunorubicin (an anthracycline) than either WT or *Idh1*^{R132};*Flt3*^{ITD} BM cells, although all three were equally sensitive to Ara-C (Fig. 6 *A* and *B*).

A more recent and targeted approach to treating *IDH*-mutated AML uses small-molecule IDH inhibitors (IDHi) in an attempt to avoid the toxicity of chemotherapy and to overcome the epigenetic effects of the mutation (12, 13). To assess IDHi efficacy in our mouse model, we transplanted CD45.2$^+$ *Idh1*^{R132};*Npm1c* AML cells into WT CD45.1$^+$ recipient mice and treated them from day 2 to 18 posttransplant with either vehicle or an amorphous solid dispersion (SDD) formulation of AG-120, an IDH1i (54). AG-120-SDD was well tolerated by the mice (as has been found in patients). Drug level and activity assessment showed that AG-120 was present at similar concentrations in plasma, BM, and spleen of the treated mice, and D-2HG blood levels were suppressed to barely detectable (Fig. 6 *C* and *D*). However, there was no significant evidence of therapeutic benefit in terms of effects on AML cell numbers in the treated mice, based on the percentage of donor-derived CD45.2$^+$ cells, relative to recipient-derived CD45.1$^+$ cells (Fig. 6*E*). This lack of effect was corroborated by histological examinations of BM and spleen from vehicle- and AG-120-SDD-treated mice (*SI Appendix*, Fig. S7*B*). Notably, however, there was a significant reduction in body weight loss in the drug-treated vs control mice (*SI Appendix*, Fig. S7*C*).

IDHi drugs work, in part, by reducing hypermethylation such that the stalled differentiation of *IDH1/2*-mutant AML cells can resume (10–12, 55–57). We therefore determined CD11b and Gr1 cell surface expression among gated CD45.2$^+$ cells isolated from our AG-120-SDD-treated *Idh1*^{R132};*Npm1c* AML mice. In the BM, spleen, and PB of the treated animals, there was a decreased proportion of immature CD11b$^-$Gr1$^-$ cells and a conversely increased proportion of CD11b$^+$Gr1$^+$ cells, in keeping with the induction of differentiation by drug treatment (Fig. 6 *F* and *G* and *SI Appendix*, Fig. S7 *D* and *E*). To further explore this finding, and because we had found that LICs were enriched in the cKit$^+$ compartment (*SI Appendix*, Fig. S4 *I–L*), we assessed the cKit$^+$ population and found that with AG-120-SDD treatment, there was reduced CD45.2$^+$ cKit$^+$ cells in BM, spleen, and PB (Fig. 6*H* and *SI Appendix*, Fig. S7 *F* and *G*). Interestingly, over the brief treatment period of 17 d, there was a significant but variable elevation in hemoglobin, as well as a trend toward increased platelets, in the treated animals (Fig. 6 *J* and *K*). However, leukocytosis and splenomegaly were not ameliorated, and mouse survival was extended only modestly (23.0 d and 26.5 d) (Fig. 6 *I* and *L* and *SI Appendix*, Fig. S7*H*).

We next turned to published data from AML patients and compared the gene expression patterns of clinical responders and nonresponders to IDHi (17). We found that the transcriptional signature associated with IDHi resistance included enrichment of interferon response genes and downregulation of genes related to heme metabolism, OXPHOS, transporter activity, and KLF1 targets (*SI Appendix*, Fig. S7*I*), a pattern shared with our murine *Idh1*^{R132};*Npm1c* cells. Together, these findings suggest that our *Idh1*^{R132};*Npm1c* mouse may be a helpful tool for examining human primary resistance to therapy targeting mutant IDH.

Therapeutic Alternatives for AML Cases that Bear *IDH* Plus *NPM1c* Mutations and Exhibit IDHi Resistance. AG-120-SDD treatment demonstrated only modest beneficial effects in *Idh1*^{R132};*Npm1c* AML mice, a situation corresponding to that of human AML that often fails to respond to IDHi. We therefore used our mouse model to investigate other therapeutic options for this subtype of AML. Because we had observed that our mouse *Idh1*^{R132};*Npm1c* BM cells were sensitive to daunorubicin in vitro (Fig. 6*A*), we chose to examine doxorubicin (Doxo), an anthracycline suitable

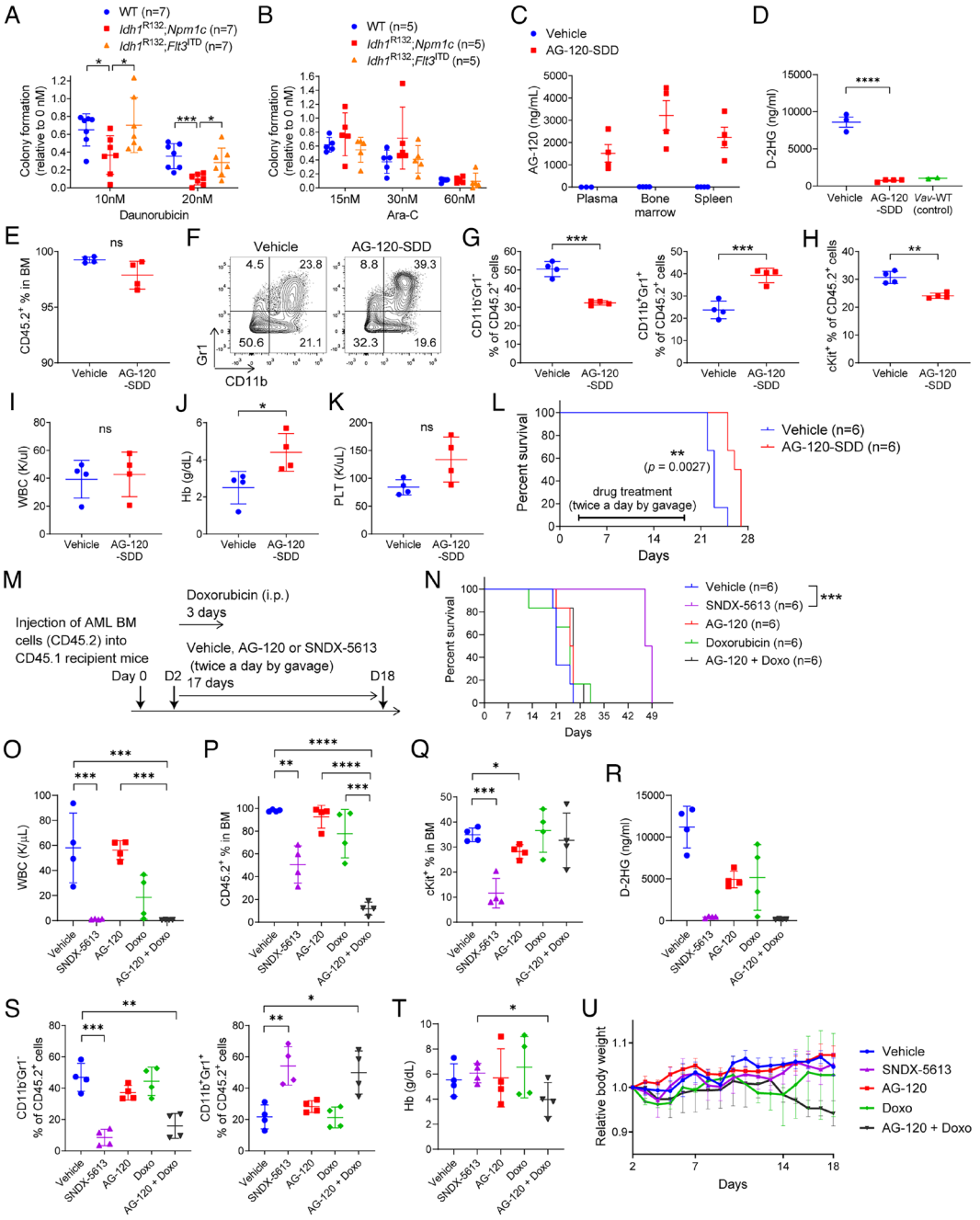

Fig. 6. Effects of combined *Idh1*^{R132} and *Npm1c* mutations on responses to chemotherapy and IDH inhibitor treatments, and potential therapeutic alternatives for mice bearing AML with *Idh* plus *Npm1c* mutations and showing IDHi resistance. (*A* and *B*) Colony formation by WT, *Idh1*^{R132};*Npm1c* and *Idh1*^{R132};*Flt3*^{ITD} BM cells that were plated in methylcellulose medium containing the indicated concentrations of (*A*) daunorubicin or (*B*) Ara-C. Data are expressed relative to untreated controls. (*C*) Quantitation of AG-120 concentrations in plasma, BM, and spleens of recipients that were transplanted with *Idh1*^{R132};*Npm1c* AML cells and treated with either vehicle or 150 mg/kg AG-120-SDD by oral gavage twice daily from day 2 to 18 (n = 3 to 4/group). (*D*) D-2HG levels in PB from the mice in *C* (n = 3 to 4/group), and untreated *Vav-Cre* WT mice (control; n = 2). (*E*) Percentage of CD45.2$^+$ (donor-derived) cells among total CD45$^+$ cells [CD45.1$^+$ (recipient-derived) cells plus CD45.2$^+$ cells] in BM from the mice in *C* (n = 4/group). (*F*) Representative FCA of CD11b and Gr1 expression among CD45.2$^+$ (donor-derived) cells in BM of the mice in *C* (n = 4/group). (*G*) Frequencies of CD11b$^-$Gr1$^-$ cells (*Left*) and CD11b$^+$Gr1$^+$ cells (*Right*) from the data in *F*. (*H*) Frequency of cKit$^+$ cells among CD45.2$^+$ (donor-derived) cells in BM of the mice in *C* (n = 4/group). (*I–K*) CBC parameters in PB from the mice in *C* (n = 4/group). WBC count (*I*), hemoglobin (Hb) levels (*J*), and platelet (PLT) counts (*K*) are shown. (*L*) Kaplan–Meier survival curves of CD45.1 recipient mice transplanted with *Idh1*^{R132};*Npm1c* AML cells and treated with either vehicle or AG-120-SDD as indicated from day 2 to 18 (n = 6/group). (*M*) Schematic diagram of experiment in which CD45.1 mice were transplanted with *Idh1*^{R132};*Npm1c* AML cells (CD45.2) and treated with either vehicle or the indicated drugs in separate cohorts. (*N*) Kaplan–Meier survival curves of the treated AML mice in *M* (n = 6/group). (*O*) WBC count on day 18 in PB from transplanted AML mice treated with the indicated drugs as in *M* (n = 4/group). (*P*) Percentage of CD45.2$^+$ (donor-derived) cells among total CD45$^+$ cells [CD45.1$^+$ (recipient-derived) cells plus CD45.2$^+$ cells] in BM from the mice in *M* (n = 4/group). (*Q*) Frequency of cKit$^+$ cells among viable cells in BM from the mice in *M* (n = 4/group). (*R*) D-2HG levels in PB from the mice in *M* (n = 4/group). (*S*) Frequencies of CD11b$^-$Gr1$^-$ cells (*Left*) and CD11b$^+$Gr1$^+$ cells (*Right*) among CD45.2$^+$ (donor-derived) cells in BM from the mice in *M* (n = 4/group). (*T*) Hb levels in the mice in M (n = 4/group). (*U*) Body weights of the mice in *M* (n = 4/group) over 18 d.

for in vivo treatment of mice (58), as well as the menin inhibitor revumenib (SNDX-5613), which is reportedly an effective therapy for human *NPM1c*-mutated AML (59). As shown in Fig. 6*M*, we treated *Idh1*^{R132};*Npm1c* AML mice with vehicle, SNDX-5613, or AG-120 (from a different supplier) twice daily by gavage over 17 d; or with Doxo once daily on days 2, 3, and 4 posttransplant; or with AG-120 plus Doxo. Interestingly, SNDX-5613 treatment significantly improved mouse survival for up to 49 d, whereas all

animals treated with the other regimens succumbed within 31 d (Fig. 6*N*). Analysis on day 18, when SNDX-5613 or AG-120 treatment was terminated, revealed that SNDX-5613 therapy had caused a reduction in leukemic burden as judged by peripheral WBC count, spleen weight, histological findings (reduced BM and liver blast infiltration), decreased proportion of CD45.2$^+$ cells (particularly cKit$^+$ cells), and a reduction in D-2HG levels (Fig. 6 *O*–*R* and *SI Appendix*, Fig. S8 *A*–*D*). Also at day 18, there was an increase in CD11b$^+$Gr1$^+$ cells demonstrating the induction of differentiation of *Idh1*^{R132};*Npm1c* cells (Fig. 6*S*), in line with previously reported responses to this drug in the clinic and in PDX mouse models (59, 60). These results indicate that SNDX-5613 treatment targeted *Idh1*^{R132};*Npm1c* AML cells in an efficient and minimally toxic way, likely through inactivation of the *Npm1c* driver effect in the double mutant cells. On its own, AG-120 had little to no effect on leukemic parameters, although there was a reduction in D-2HG levels (Fig. 6 *O*–*R* and *SI Appendix*, Fig. S8 *A*–*D*). While single agent Doxo had inconsistent effects on leukemic parameters and D-2HG levels, AG-120 plus Doxo reduced spleen weight, eliminated infiltrating cells in BM and liver, and decreased D-2HG levels equivalent to those achieved with SNDX-5613 treatment. However, these positive changes were not associated with improved survival of the mice. All mice treated with AG-120 plus Doxo developed anemia and a dramatic decrease in weight (Fig. 6 *T* and *U*), with all animals dying by day 29 (Fig. 6*N*). It appears that this combination therapy, while effective in killing the *Idh1*^{R132};*Npm1c* cells, produced unexpected toxicity that resulted in the death of the animals.

Discussion

Until now, there has been a lack of an *IDH1*-mutant mouse model that develops overt AML and is useful for studying the effects of combining *IDH1* mutations with other driver mutations. We have filled this gap with our *Vav-Cre* conditional double knock-in *Idh1*^{R132};*Npm1c* mouse, which recapitulates critical features of the corresponding human AML disease in terms of gross phenotype and molecular signature, as well as sensitivity and response to therapeutic agents. These animals therefore provide the field with a potentially valuable resource for increasing our understanding of AML biology. Importantly, we have demonstrated through in vivo use of AG-120, SNDX-5613, and Doxo that our AML mouse model can facilitate the testing of drugs as single agents or in combination. These animals can also be utilized for future studies aimed at understanding the underlying mechanisms of treatment resistance and how to overcome them.

The models presented here have provided important insights into the individual and cooperative roles of *Idh1* mutations with mutations of *Npm1c* or *Flt3*^{ITD} (*SI Appendix*, Fig. S9). We observed that *Idh1* mutations on their own had little effect on normal blood cell production, consistent with findings in humans with an acquired *IDH1* mutation. In contrast, the presence of an *Npm1c* or *Flt3*^{ITD} mutation in our mice was associated with an increased WBC, anemia, and thrombocytopenia. Notably, marked thrombocytopenia was present in *Npm1c* mice from the earliest observation point, consistent with a major effect of this mutation being to block normal myeloid differentiation. *Npm1c* mutations also affected WBC differentiation, as seen in the altered CD11b/Gr1 expression pattern in *Npm1c* and *Idh1*^{R132};*Npm1c* mice.

Our gene expression and epigenetic studies identified significantly different alterations to hematopoiesis in mice bearing *Npm1c* and *Flt3*^{ITD} mutations, with or without *Idh1* mutation; this result highlights the modifying, but not primary, role of the *Idh1* mutation in the disease phenotype. In our *Flt3*^{ITD} mice from the earliest time point assessed (3 mo), there was decreased expression of pathways in heme metabolism, transporter activity, and KLF1 downstream target genes. These changes were independent of the *Idh1* mutation and likely account for the anemia seen in these animals. The presence of the *Npm1c* mutation had broader effects, namely increased expression of immune response genes (including interferons) as well as decreased expression of respiratory chain and oxidative phosphorylation programs. Interestingly, in mice where the *Npm1c* mutation was combined with the *Idh1* mutation, there was decreased expression of heme metabolism, transporter, and KLF1 target genes. These changes can explain the observation that anemia was enhanced in *Idh1*^{R132};*Npm1c* mice compared to *Npm1c* mice.

A more in-depth analysis of gene expression revealed that there was a greater degree of up- and downregulation of genes in *Flt3*^{ITD} mice than in *Npm1c* mice, likely reflecting the signaling nature of the *Flt3*^{ITD} mutation and the activation of the pSTAT5 pathway by this kinase. With regard to genes affected by the *Flt3*^{ITD} mutation, several stood out. For example, there was reduced expression of the differentiation antigens *Pax5* and *Gata1*, and increased expression of *Il2ra*, *Socs2,* and *Socs2-AS1*. Upregulation of these latter genes has been associated with poor clinical outcomes in human AML (41–43), a link that can now be explored further using our models. For mice with a *Npm1c* mutation, there was prominent activation of expression of Hox family members, a key feature of *NPM1c* mutant AML (26, 40).

AML is both a genetic and epigenetic disease. Interestingly, and in keeping with the function of IDH1, the combination of mutant *Idh1* with *Npm1c* or *Flt3*^{ITD} was associated with loss of hypomethylated sites (Fig. 5). Although the combination of *Idh1*^{R132} with mutant *Npm1c* enhanced the block in AML blast cell differentiation, the in vivo treatment of mice bearing *Idh*^{R132};*Npm1c* AML cells with AG-120-SDD had only a modest effect on hemoglobin, mature myeloid cells, and platelet count, despite a marked reduction in D-2HG levels. This failure of a more robust response may be due to the relatively short period of treatment (17 d). Alternatively, the cells may have acquired secondary mutations that rendered them resistant to the effects of the inhibitor. Further studies with prolonged drug exposure and molecular analyses of the persistent cells will be required to resolve this issue. Importantly, our model did demonstrate that the menin inhibitor SNDX-5613 was effective in eliminating *Idh1*^{R132};*Npm1c* cells, likely through its effects on the leukemia driver *Npm1c*.

Among the three hot spot mutations of the *IDH* genes, *IDH1*^{R132} and *IDH2*^{R140} have been demonstrated to be similar in terms of biological effects, as well as their co-occurrence with *NPM1c*, in contrast to the uniqueness of the *IDH2*^{R172} mutation and its very rare co-occurrence with *NPM1c* (5, 61–64). Based on these considerations, studies using *IDH1*^{R132} knock-in mice particularly with regard to cooperation with *NPM1c*, are likely to be relevant to the *IDH2*^{R140} mutation, although formal confirmation is required.

In conclusion, our study has described the disease phenotypes developing in two different mouse models based on the oncogenes *Npm1c* and *Flt3*^{ITD} either alone or when coexpressed with the *Idh1*^{R132} mutation. A limitation of these models is that the mutant forms are present from the time of birth, rather than being acquired individually over time. Despite this, many characteristics of human disease were replicated in our models, making them suitable for future explorations of the mechanisms linked to these cooperating oncogenic events as well as for the testing of novel drug combinations. The fact that the disease developed in immune-competent

animals is significant, providing a resource to explore how these genetic changes can modify the animal, allowing for the development of myeloproliferative diseases and leukemia.

Materials and Methods

A full description of Materials and Methods is provided in *SI Appendix*.

Mice. The generation of *Idh1*^{R132H} conditional knock-in (*Idh1*-LSL-R132H) mice was described previously (63). Conditional *Npm1*$^{flox\text{-}cA/+}$ mice were kindly provided by George S. Vassiliou (Wellcome Trust Sanger Institute, Cambridge, UK) (26). *Flt3*^{ITD} knock-in mice were previously described (27) and obtained from the Jackson Laboratory (B6.129-*Flt3*^{tm1Dgg}/J, #011112, RRID: IMSR_JAX:011112). *Vav-Cre* mice (#008610, RRID: IMSR_JAX:008610) and CD45.1 mice (#002014, RRID: IMSR_JAX:002014) were from the Jackson Laboratory. All animal experiments were approved by the University Health Network Animal Care Committee (University Health Network, Princess Margaret Cancer Centre, protocol #985, #6694).

Data, Materials, and Software Availability. All data generated from the mice in this study have been deposited in the Gene Expression Omnibus under series accession number GSE215370 (65) as well as GSE215369 (66) (RNA-seq), GSE215367 (67) (ATAC-seq), and GSE215368 (68) (bisulfite-seq).

ACKNOWLEDGMENTS. This work was supported by grants from the Leukemia and Lymphoma Society (LLS 7029-22) (to R.L.L., A.M.M., C.E.M., M.D.M., and T.W.M.); from the Canadian Institutes of Health Research (RN482269–480701) (to T.W.M.); from the Centre for Oncology and Immunology under the Health@InnoHK Initiative funded by the Innovation and Technology Commission, the Government of Hong Kong SAR, China (to T.W.M.); from the National Cancer Institute (K99CA248460) (to R.L.B.); from JSPS KAKENHI (20K17377) (to T.S.). J.L. was supported by a Cancer Research Institute Irvington Fellowship from the Cancer Research Institute. Work in the Levine Lab was supported by NCI 2P30CA008748-48 (MSK Cancer Center Support Grant). C.E.M. and Cornell would like to thank the Scientific Computing Unit (SCU) and the Starr Cancer Consortium (I7-A765, I9-A9-071, I13-0052), and gratefully acknowledge funding from the Vallee Foundation, the WorldQuant Foundation, The Pershing Square Sohn Cancer Research Alliance, the NIH (R01MH117406, R01CA249054, R01AI151059, P01CA214274), and the Leukemia and Lymphoma Society (LLS 9238-16, LLS-MCL-982). In addition, we thank the staff members of the Princess Margaret Cancer Centre Flow Cytometry Facility, Histology Facility, and Animal Resource Centre for their services; and the staff of the Weill Cornell Medicine Epigenetics Core for technical support. Finally, we appreciate the administrative assistance of Irene Ng and the scientific editing of Mary Saunders. S.M.C. receives unrelated research funding from Servier, AbbVie, and Celgene/BMS. R.L.L. receives research support from Ajax and Abbvie.

Author affiliations: [a]Princess Margaret Cancer Centre, University Health Network, Toronto, ON M5G 2C1, Canada; [b]Department of Hematology, Graduate School of Medicine, Kyoto University, Kyoto 606-8507, Japan; [c]BMP, Ecosystem, stemness and dynamic in cancer Laboratory, Centre de Recherche en Cancerologie de Lyon, UMR INSERM 1052 CNRS 5286, Centre Léon Bérard, Université Claude Bernard Lyon 1, Lyon 69008, France; [d]Department of Physiology and Biophysics, Weill Cornell Medicine, New York, NY 10065; [e]The HRH Prince Alwaleed Bin Talal Bin Abdulaziz Alsaud Institute for Computational Biomedicine, Weill Cornell Medicine, New York, NY 10065; [f]WorldQuant Initiative for Quantitative Prediction, Weill Cornell Medicine, New York, NY 10065; [g]Department of Medicine, Division of Hematology and Medical Oncology, Weill Cornell Medicine, New York, NY 10021; [h]Department of Neurology and Neurosurgery, McGill University, Montréal, QC H3A 1A1, Canada; [i]Division of Cellular Signaling, National Cancer Center Research Institute, Tokyo 104-0045, Japan; [j]Centre for Oncology and Immunology, Hong Kong Science Park, Hong Kong SAR, China; [k]Institut Mondor de Recherche Biomédicale, INSERM U955, Université Paris Est Créteil, Créteil 94010, France; [l]Department of Pathology, Cancer University Institute of Toulouse-Oncopole, University Hospital of Toulouse, INSERM U1037, Cancer Research Center in Toulouse, Toulouse 31059, France; [m]Human Oncology and Pathogenesis Program, Memorial Sloan Kettering Cancer Center, New York, NY 10065; [n]Agios Pharmaceuticals, Cambridge, MA 02139; [o]Center for Epigenetics Research, Memorial Sloan Kettering Cancer Center, New York, NY 10065; [p]Center for Hematologic Malignancies, Memorial Sloan Kettering Cancer Center, New York, NY 10065; and [q]Department of Pathology, School of Clinical Medicine, Li Ka Shing Faculty of Medicine, The University of Hong Kong, Hong Kong SAR, China

Author contributions: T.S., J.L., X.Z., T.B., J. Fortin, S.M.C., M.-F.C., S.I., F.L., R.L.L., A.M.M., C.E.M., M.D.M., and T.W.M. designed research; T.S., J.L., X.Z., C.M., J. Foox, P.R., L.D.H., W.Z., T.B., J. Fortin, S.M.C., M.-F.C., S.I., W.Y.L., M.F.C., G.S.D., A.W., C.T., R.M., I.C., C.B., S.M.J., R.L.B., B.N., S.R., and R.N. performed research; T.S., S.M.C., R.L.B., R.L.L., A.M.M., C.E.M., M.D.M., and T.W.M. contributed new reagents/analytic tools; T.S., J.L., X.Z., C.M., J. Foox, P.R., L.D.H., W.Z., T.B., J. Fortin, S.M.C., M.-F.C., S.I., W.Y.L., M.F.C., C.T., C.B., R.L.B., B.N., S.R., R.N., R.L.L., A.M.M., C.E.M., and T.W.M. analyzed data; and T.S., J.L., X.Z., C.M., J. Foox, P.R., L.D.H., T.B., J. Fortin, S.M.C., S.I., W.Y.L., F.L., C.B., R.L.B., R.L.L., A.M.M., C.E.M., M.D.M., and T.W.M. wrote the paper.

1. J. P. Patel *et al.*, Prognostic relevance of integrated genetic profiling in acute myeloid leukemia. *N. Engl. J. Med.* **366**, 1079–1089 (2012).
2. The Cancer Genome Atlas Research Network, Genomic and epigenomic landscapes of adult de novo acute myeloid leukemia. *N. Engl. J. Med.* **368**, 2059–2074 (2013).
3. B. J. Wouters, R. Delwel, Epigenetics and approaches to targeted epigenetic therapy in acute myeloid leukemia. *Blood* **127**, 42–52 (2016).
4. K. H. Metzeler *et al.*, Spectrum and prognostic relevance of driver gene mutations in acute myeloid leukemia. *Blood* **128**, 686–698 (2016).
5. E. Papaemmanuil *et al.*, Genomic classification and prognosis in acute myeloid leukemia. *N. Engl. J. Med.* **374**, 2209–2221 (2016).
6. J. W. Tyner *et al.*, Functional genomic landscape of acute myeloid leukaemia. *Nature* **562**, 526–531 (2018).
7. R. A. Cairns, T. W. Mak, Oncogenic isocitrate dehydrogenase mutations: Mechanisms, models, and clinical opportunities. *Cancer Discov.* **3**, 730–741 (2013).
8. M. E. Figueroa *et al.*, Leukemic IDH1 and IDH2 mutations result in a hypermethylation phenotype, disrupt TET2 function, and impair hematopoietic differentiation. *Cancer Cell* **18**, 553–567 (2010).
9. C. Lu *et al.*, IDH mutation impairs histone demethylation and results in a block to cell differentiation. *Nature* **483**, 474–478 (2012).
10. F. Wang *et al.*, Targeted inhibition of mutant IDH2 in leukemia cells induces cellular differentiation. *Science* **340**, 622–626 (2013).
11. A. H. Shih *et al.*, Combination targeted therapy to disrupt aberrant oncogenic signaling and reverse epigenetic dysfunction in IDH2- and TET2-mutant acute myeloid leukemia. *Cancer Discov.* **7**, 494–505 (2017).
12. E. M. Stein *et al.*, Enasidenib in mutant IDH2 relapsed or refractory acute myeloid leukemia. *Blood* **130**, 722–731 (2017).
13. C. D. DiNardo *et al.*, Durable remissions with ivosidenib in IDH1-mutated relapsed or refractory AML. *N. Engl. J. Med.* **378**, 2386–2398 (2018).
14. J. J. Harding *et al.*, Isoform switching as a mechanism of acquired resistance to mutant isocitrate dehydrogenase inhibition. *Cancer Discov.* **8**, 1540–1547 (2018).
15. A. M. Intlekofer *et al.*, Acquired resistance to IDH inhibition through trans or cis dimer-interface mutations. *Nature* **559**, 125–129 (2018).
16. S. Choe *et al.*, Molecular mechanisms mediating relapse following ivosidenib monotherapy in IDH1-mutant relapsed or refractory AML. *Blood Adv.* **4**, 1894–1905 (2020).
17. F. Wang *et al.*, Leukemia stemness and co-occurring mutations drive resistance to IDH inhibitors in acute myeloid leukemia. *Nat. Commun.* **12**, 2607 (2021).
18. A. C. H. Liu *et al.*, Targeting STAT5 signaling overcomes resistance to IDH inhibitors in acute myeloid leukemia through suppression of stemness. *Cancer Res.* **82**, 4325–4339 (2022).
19. J. Lyu *et al.*, Disabling uncompetitive inhibition of oncogenic IDH mutations drives acquired resistance. *Cancer Discov.* **13**, 170–193 (2023).
20. S. Inoue *et al.*, Mutant IDH1 downregulates ATM and alters DNA repair and sensitivity to DNA damage independent of TET2. *Cancer Cell* **30**, 337–348 (2016).
21. M. Sasaki *et al.*, IDH1(R132H) mutation increases murine haematopoietic progenitors and alters epigenetics. *Nature* **488**, 656–659 (2012).
22. A. Yeaton *et al.*, The impact of inflammation-induced tumor plasticity during myeloid transformation. *Cancer Discov.* **12**, 2392–2413 (2022).
23. B. Falini *et al.*, Cytoplasmic nucleophosmin in acute myelogenous leukemia with a normal karyotype. *N. Engl. J. Med.* **352**, 254–266 (2005).
24. H. Dohner *et al.*, Diagnosis and management of AML in adults: 2017 ELN recommendations from an international expert panel. *Blood* **129**, 424–447 (2017).
25. H. Dohner *et al.*, Diagnosis and management of AML in adults: 2022 recommendations from an international expert panel on behalf of the ELN. *Blood* **140**, 1345–1377 (2022).
26. G. S. Vassiliou *et al.*, Mutant nucleophosmin and cooperating pathways drive leukemia initiation and progression in mice. *Nat. Genet.* **43**, 470–475 (2011).
27. B. H. Lee *et al.*, FLT3 mutations confer enhanced proliferation and survival properties to multipotent progenitors in a murine model of chronic myelomonocytic leukemia. *Cancer Cell* **12**, 367–380 (2007).
28. M. Mallardo *et al.*, NPMc+ and FLT3_ITD mutations cooperate in inducing acute leukaemia in a novel mouse model. *Leukemia* **27**, 2248–2251 (2013).
29. A. Mupo *et al.*, A powerful molecular synergy between mutant Nucleophosmin and Flt3-ITD drives acute myeloid leukemia in mice. *Leukemia* **27**, 1917–1920 (2013).
30. A. H. Shih *et al.*, Mutational cooperativity linked to combinatorial epigenetic gain of function in acute myeloid leukemia. *Cancer Cell* **27**, 502–515 (2015).
31. U. Testa, G. Castelli, E. Pelosi, Isocitrate dehydrogenase mutations in myelodysplastic syndromes and in acute myeloid leukemias. *Cancers* **12**, 2427 (2020).
32. L. Quek *et al.*, Clonal heterogeneity of acute myeloid leukemia treated with the IDH2 inhibitor enasidenib. *Nat. Med.* **24**, 1167–1177 (2018).
33. G. J. Roboz *et al.*, Ivosidenib induces deep durable remissions in patients with newly diagnosed IDH1-mutant acute myeloid leukemia. *Blood* **135**, 463–471 (2020).
34. A. J. Deshpande *et al.*, Acute myeloid leukemia is propagated by a leukemic stem cell with lymphoid characteristics in a mouse model of CALM/AF10-positive leukemia. *Cancer Cell* **10**, 363–374 (2006).
35. K. Petropoulos *et al.*, A novel role for Lef-1, a central transcription mediator of Wnt signaling, in leukemogenesis. *J. Exp. Med.* **205**, 515–522 (2008).
36. C. T. Collins, J. L. Hess, Role of HOXA9 in leukemia: Dysregulation, cofactors and essential targets. *Oncogene* **35**, 1090–1098 (2016).

37. I. Khan, M. A. Amin, E. A. Eklund, A. L. Gartel, Regulation of HOX gene expression in AML. *Blood Cancer J.* **14**, 42 (2024).
38. S. E. Meyer *et al.*, DNMT3A haploinsufficiency transforms FLT3ITD myeloproliferative disease into a rapid, spontaneous, and fully penetrant acute myeloid leukemia. *Cancer Discov.* **6**, 501–515 (2016).
39. M. Siatecka, J. J. Bieker, The multifunctional role of EKLF/KLF1 during erythropoiesis. *Blood* **118**, 2044–2054 (2011).
40. H. J. Uckelmann *et al.*, Therapeutic targeting of preleukemia cells in a mouse model of NPM1 mutant acute myeloid leukemia. *Science* **367**, 586–590 (2020).
41. S. W. Ng *et al.*, A 17-gene stemness score for rapid determination of risk in acute leukaemia. *Nature* **540**, 433–437 (2016).
42. C. H. Nguyen *et al.*, IL2RA promotes aggressiveness and stem cell-related properties of acute myeloid leukemia. *Cancer Res.* **80**, 4527–4539 (2020).
43. R. Zhang, C. H. Huo, Long noncoding RNA SOCS2-AS promotes leukemogenesis in FLT3-ITD+ acute myeloid leukemia through miRNA-221. *OncoTargets Ther.* **13**, 2925–2934 (2020).
44. S. C. Kogan *et al.*, Bethesda proposals for classification of nonlymphoid hematopoietic neoplasms in mice. *Blood* **100**, 238–245 (2002).
45. A. Zehir *et al.*, Mutational landscape of metastatic cancer revealed from prospective clinical sequencing of 10,000 patients. *Nat. Med.* **23**, 703–713 (2017).
46. J. L. Patel *et al.*, Coexisting and cooperating mutations in NPM1-mutated acute myeloid leukemia. *Leukemia Res.* **56**, 7–12 (2017).
47. A. V. Krivtsov *et al.*, Transformation from committed progenitor to leukaemia stem cell initiated by MLL-AF9. *Nature* **442**, 818–822 (2006).
48. P. Kirstetter *et al.*, Modeling of C/EBPalpha mutant acute myeloid leukemia reveals a common expression signature of committed myeloid leukemia-initiating cells. *Cancer Cell* **13**, 299–310 (2008).
49. P. Zhang *et al.*, Dietary intake of fructose increases purine de novo synthesis: A crucial mechanism for hyperuricemia. *Front. Nutr.* **9**, 1045805 (2022).
50. S. Schnittger *et al.*, IDH1 mutations are detected in 6.6% of 1414 AML patients and are associated with intermediate risk karyotype and unfavorable prognosis in adults younger than 60 years and unmutated NPM1 status. *Blood* **116**, 5486–5496 (2010).
51. F. Vergez *et al.*, Phenotypically-defined stages of leukemia arrest predict main driver mutations subgroups, and outcome in acute myeloid leukemia. *Blood Cancer J.* **12**, 117 (2022).
52. A. Carey *et al.*, Identification of interleukin-1 by functional screening as a key mediator of cellular expansion and disease progression in acute myeloid leukemia. *Cell Rep.* **18**, 3204–3218 (2017).
53. S. E. Kurtz *et al.*, Associating drug sensitivity with differentiation status identifies effective combinations for acute myeloid leukemia. *Blood Adv.* **6**, 3062–3067 (2022).
54. E. Gruber *et al.*, Inhibition of mutant IDH1 promotes cycling of acute myeloid leukemia stem cells. *Cell Rep.* **40**, 111182 (2022).
55. U. C. Okoye-Okafor *et al.*, New IDH1 mutant inhibitors for treatment of acute myeloid leukemia. *Nat. Chem. Biol.* **11**, 878–886 (2015).
56. K. Yen *et al.*, AG-221, a first-in-class therapy targeting acute myeloid leukemia harboring oncogenic IDH2 mutations. *Cancer Discov.* **7**, 478–493 (2017).
57. M. D. Amatangelo *et al.*, Enasidenib induces acute myeloid leukemia cell differentiation to promote clinical response. *Blood* **130**, 732–741 (2017).
58. J. Zuber *et al.*, Mouse models of human AML accurately predict chemotherapy response. *Genes Dev.* **23**, 877–889 (2009).
59. G. C. Issa *et al.*, The menin inhibitor revumenib in KMT2A-rearranged or NPM1-mutant leukaemia. *Nature* **615**, 920–924 (2023).
60. A. V. Krivtsov *et al.*, A menin-MLL inhibitor induces specific chromatin changes and eradicates disease in models of MLL-rearranged leukemia. *Cancer Cell* **36**, 660–673.e11 (2019).
61. P. S. Ward *et al.*, The potential for isocitrate dehydrogenase mutations to produce 2-hydroxyglutarate depends on allele specificity and subcellular compartmentalization. *J. Biol. Chem.* **288**, 3804–3815 (2013).
62. F. Lemonnier *et al.*, The IDH2 R172K mutation associated with angioimmunoblastic T-cell lymphoma produces 2HG in T cells and impacts lymphoid development. *Proc. Natl. Acad. Sci. U.S.A.* **113**, 15084–15089 (2016).
63. J. Fortin *et al.*, Distinct and opposite effects of leukemogenic Idh and Tet2 mutations in hematopoietic stem and progenitor cells. *Proc. Natl. Acad. Sci. U.S.A.* **120**, e2208176120 (2023).
64. M. Meggendorfer *et al.*, IDH1R132, IDH2R140 and IDH2R172 in AML: Different genetic landscapes correlate with outcome and may influence targeted treatment strategies. *Leukemia* **32**, 1249–1253 (2018).
65. C. Meydan *et al.*, Mutant IDH1 cooperates with NPM1c or FLT3-ITD to drive distinct myeloid diseases and molecular outcomes. Gene Expression Omnibus. https://www.ncbi.nlm.nih.gov/geo/query/acc.cgi?acc=GSE215370. Deposited 12 October 2022.
66. T. Sakamoto *et al.*, Mutant IDH1 cooperates with NPM1c or FLT3-ITD to drive distinct myeloid diseases and molecular outcomes. Gene Expression Omnibus. https://www.ncbi.nlm.nih.gov/geo/query/acc.cgi?acc=GSE215369. Deposited 12 October 2022.
67. T. Sakamoto *et al.*, Mutant IDH1 cooperates with NPM1c or FLT3-ITD to drive distinct myeloid diseases and molecular outcomes. Gene Expression Omnibus. https://www.ncbi.nlm.nih.gov/geo/query/acc.cgi?acc=GSE215367. Deposited 12 October 2022.
68. T. Sakamoto *et al.*, Mutant IDH1 cooperates with NPM1c or FLT3-ITD to drive distinct myeloid diseases and molecular outcomes. Gene Expression Omnibus. https://www.ncbi.nlm.nih.gov/geo/query/acc.cgi?acc=GSE215368. Deposited 12 October 2022.